

Sociology and hierarchy of voids: A study of seven nearby CAVITY galaxy voids and their dynamical CosmicFlows-3 environment

H.M. Courtois^{*1}, R. van de Weygaert², M. Aubert¹, D. Pomarède³, D. Guinet¹, J. Domínguez-Gómez⁴, E. Florido^{4,5}, L. Galbany^{6,7}, R. García-Benito⁸, J.M. van der Hulst², K. Kreckel⁹, R.E. Miura^{4,10}, I. Pérez^{4,5}, S. Planelles^{11,12}, V. Quilis^{11,12}, J. Román^{2,13,14}, and M. Sánchez-Portal¹⁵

¹ Université Claude Bernard Lyon 1, IUF, IP2I Lyon, 69622 Villeurbanne, France

² Kapteyn Astronomical Institute, University of Groningen, PO Box 800, 9700 AV Groningen, The Netherlands

³ IRFU, CEA Université Paris-Saclay, 91191 Gif-sur-Yvette, France

⁴ Departamento de Física Teórica y del Cosmos, Campus de Fuente Nueva, Edificio Mecenaz, Universidad de Granada, E-18071, Granada, Spain

⁵ Instituto Carlos I de Física Teórica y Computacional, Facultad de Ciencias, E-18071 Granada, Spain

⁶ Institute of Space Sciences (ICE, CSIC), Campus UAB, Carrer de Can Magrans, s/n, E-08193 Barcelona, Spain

⁷ Institut d'Estudis Espacials de Catalunya (IEEC), E-08034 Barcelona, Spain

⁸ Instituto de Astrofísica de Andalucía - CSIC Glorieta de la Astronomía E-18008, Granada, Spain

⁹ Astronomisches Rechen-Institut, Zentrum für Astronomie der Universität Heidelberg, Mönchhofstrasse 12-14, D-69120 Heidelberg, Germany

¹⁰ National Astronomical Observatory of Japan, National Institutes of Natural Sciences, 2-21-1 Osawa, Mitaka, Tokyo 181-8588, Japan

¹¹ Departamento de Astronomía y Astrofísica, Universidad de Valencia, c/ Dr. Moliner n 50, 46100 - Burjassot (Valencia), Spain

¹² Observatori Astronòmic, Universitat de València, E-46980 Paterna (València), Spain

¹³ Departamento de Astrofísica, Universidad de La Laguna, E-38206, La Laguna, Tenerife, Spain

¹⁴ Instituto de Astrofísica de Canarias, c/ Vía Láctea s/n, E-38205, La Laguna, Tenerife, Spain

¹⁵ Institut de Radioastronomie Millimétrique (IRAM), Av. Divina Pastora 7, Local 20, 18012 Granada, Spain

Received A&A Nov 29, 2022 - AA/2022/45578 / Accepted March 3rd, 2023

ABSTRACT

Context. The present study addresses a key question related to our understanding of the relation between void galaxies and their environment: the relationship between luminous and dark matter in and around voids.

Aims. To explore the extent to which local Universe voids are empty of matter, we study the full (dark+luminous) matter content of seven nearby cosmic voids that are fully contained within the CosmicFlows-3 volume.

Methods. We obtained the matter-density profiles of seven cosmic voids using two independent methods. These were built from the galaxy redshift space two-point correlation function in conjunction with peculiar velocity gradients from the CosmicFlows-3 dataset.

Results. The results are striking, because when the redshift survey is used, all voids show a radial positive gradient of galaxies, while based on the dynamical analysis, only three of these voids display a clear underdensity of matter in their center.

Conclusions. This work constitutes the most detailed observational analysis of voids conducted so far, and shows that void emptiness should be derived from dynamical information. From this limited study, the Hercules void appears to be the best candidate for a local Universe pure "pristine volume", expanding in three directions with no dark matter located in that void.

Key words. Cosmology: large-scale structure of Universe

1. Introduction

Galaxies are not evenly distributed in space. Instead, they probe the underlying inhomogeneous dark matter distribution. On megaparsec scales, matter and galaxies are organized in a web-like network called the cosmic web (Bond et al. 1996; Cautun et al. 2014). Prominent elongated filaments define a pervasive structure that assembles most of the matter and galaxies in the Universe and form intergalactic transport channels along which mass is migrating towards the dense, compact clusters and the nodes of the web. An equally outstanding aspect of the web-like cosmic mass distribution is the nearly empty void regions (e.g., Kirshner et al. 1981; de Lapparent et al. 1986; Huchra et al.

2012). These are enormous regions with sizes in the range of $20\text{--}50h^{-1}$ Mpc that are significantly less populated with galaxies than filaments and clusters. Voids are generally roundish in shape and occupy the major share of space (see e.g., van de Weygaert & Platen 2011; van de Weygaert 2016, for reviews), assuming around 75% – 80% of it (e.g., Cautun et al. 2014).

The dominant voids in the cosmic matter distribution are manifestations of the cosmic-structure-formation process transiting to the nonlinear stage of evolution (Blumenthal et al. 1992; Sheth & van de Weygaert 2004). Their effective repulsive influence over the surroundings has even been recognized in the CosmicFlows, which are peculiar velocity surveys of the Local Universe (Courtois et al. 2012; Tully et al. 2014). The expansion of the voids makes them organizing elements of the large-scale matter distribution, meaning they play an essential role in arrang-

* helene.courtois@univ-lyon1.fr

ing matter concentrations into an all-pervasive cosmic network (e.g., Icke 1984; Sheth & van de Weygaert 2004; Aragon-Calvo & Szalay 2013).

Many recent studies followed up on the realization that voids not only represent a key constituent of the cosmic-mass distribution, but are also one of the most direct probes of global cosmology (Goldberg & Vogeley 2004; Park & Lee 2007; Lavaux & Wandelt 2012; Bos et al. 2012; Pisani et al. 2015; Hamaus et al. 2016; Cai et al. 2015; Perico et al. 2019). Of particular interest is the realization that their structure, morphology, and dynamics reflect the nature of dark energy, dark matter, and of the possibly non-Gaussianity of the primordial perturbation field (see Pisani et al. 2019, for a review). The effects of dark energy and possible modifications of General Relativity manifest themselves more prominently in the low-density interior of voids.

The interior of voids also offer a unique testing ground for studying environmental influences on galaxy formation and evolution (Peebles 2001; Rojas et al. 2004, 2005; Kreckel et al. 2011, 2012). The low-density interior of a void is a largely pristine cosmic environment that still retains the memory of the initial conditions of the Universe soon after the big bang, and is unaffected by virialization or other effects related to gravitational collapse. Equivalent to a lower Ω_m universe (Goldberg & Vogeley 2004), galaxies in voids are expected to evolve more slowly and have a "calmer" merging history (also see Lackner et al. 2012). As a result, they appear to have significantly different properties from average field galaxies.

In general, void galaxies are small, faint, and blue galaxies (Kreckel et al. 2011) that appear to reside in a more youthful state of star formation than galaxies in denser environments (Beygu et al. 2016; Domínguez-Gómez et al. 2022). Nonetheless, while these trends appear to be quite general, controversy persists in the literature as to whether or not galaxies in voids genuinely differ in their internal properties from similar objects in denser regions. For example, while Rojas et al. (2005) found evidence for a significantly higher specific star formation rate for void galaxies, other studies (Beygu et al. 2016, e.g.) did not find evidence that void galaxies have star formation rates in excess of what might be expected for their small mass. It is a well-established fact that there are systematic differences in the masses of halos and galaxies residing in different cosmic-web environments: with respect to the generic filament environment of galaxies, the void galaxy population mass function is shifted to lower masses and lower number densities (Cautun et al. 2014; Ganeshiah Veena et al. 2019; Hellwing et al. 2021, see e.g.). A key question pertains to whether the observed systematic differences between galaxies in voids, filaments, walls, and clusters are only due to the differences in their mass, with other noticeable differences solely a direct consequence of this, or there are environment-specific factors at play (see e.g., Borzyszkowski et al. 2017; Hellwing et al. 2021). In a recent study, Goh et al. (2019) argued in favor of mass being the sole determining factor. On the other hand, specifically in the case of void galaxies, Peebles (2001), in his seminal study on the "void phenomenon", pointed out the unexpected low abundance of low-mass and dwarf galaxies in voids. This appears to be difficult to reconcile with mere mass scaling within standard LCDM cosmology and may be the strongest indication of specific void environmental processes. Indeed, there are many additional environmental factors and processes that one might expect to contribute to the outcome of the galaxy-formation process. For example, a prominent environmental influence is that of the different external tidal forces exerted on a forming halo and galaxy (see e.g., van de Weygaert & Babul 1994; Hahn et al. 2007; Yan et al. 2013;

Borzyszkowski et al. 2017; Paranjape et al. 2018; Verza et al. 2022).

With the purpose of investigating systematic differences between void galaxies and galaxies in denser environments, the Void Galaxy Survey (VGS) (Kreckel et al. 2011, 2012; Beygu et al. 2016, 2017) carried out a multi-wavelength study of about 60 void galaxies. Each galaxy was selected from the deepest interior regions of identified voids in the The Sloan Digital Sky Survey (SDSS) redshift survey on the basis of a geometric-topological watershed technique (Platen et al. 2007), with no a priori selection of intrinsic properties of the void galaxies. These authors studied the gas content, star formation history, and stellar content in detail, as well as the kinematics and dynamics of void galaxies and their companions. One of the most tantalizing findings of the VGS is the possible evidence for cold-gas accretion in some of the most interesting objects, amongst which are a polar ring galaxy and a filamentary configuration of void galaxies.

The Calar Alto Void Integral-field Treasury survey (CAVITY¹; (Pérez & al. 2023)) is the sequel to the VGS and extends the scope of the observational study of the void galaxies. The CAVITY project concentrates on the determination of the influence of the cosmic environment on galaxy formation and the mass-assembly history of void galaxies, and in particular on the drivers of galaxy transformation in voids. Insight into the dynamical state of the voids in which galaxies are located and, in particular, a sound understanding of the local relation between their dark matter and luminous matter contents are of utmost importance for a reliable interpretation of measurements of void galaxies.

The present study addresses a key open question related to our understanding of the link between void galaxies and their environment, namely the relationship between luminous and dark matter in and around voids. To this end, we seek to relate the galaxy distribution in and around a sample of nearby voids with a dynamical study of these voids. Our dynamical study is based on peculiar velocity measurements provided by the CosmicFlows-3 survey (CF3 ; (Tully et al. 2016)). We use this information to analyze the emptiness of these seven nearby (low-redshift) CAVITY voids, and to assess the corresponding relationship to the void galaxy environment.

2. Data: CAVITY and CosmicFlows-3

The CAVITY project targets void member galaxies spread across 15 singular voids. The seven voids analyzed here are taken from the CAVITY void sample on the basis of them being located in the CosmicFlows-3 reconstructed volume of the Local Universe. We use the number label that was given by (Pan et al. 2012) in order to refer to these seven voids in the present article, namely 355, 439, 474, 487, 727, 738, and 941.

2.1. CAVITY

Calar Alto Observatory selected the CAVITY project as one of the three Legacy projects that will define the Calar Alto Observatory science and technology horizon for the coming years. The CAVITY project main goals are to determine the influence of the environment on the mass assembly of void galaxies, to establish how galaxy formation depends on the larger-scale environment, and to identify the main driver of galaxy transformation in voids.

¹ <https://CAVITY.caha.es/>

To carry out this detailed study, the CAVITY galaxy sample was selected using the Catalogue of Cosmic Voids based on SDSS DR7 data (Pan et al. 2012). The selected redshift range is between 0.005 and 0.05 in order to obtain photometric and spectroscopic data reaching high-angular-resolution and faint galaxies in order to have a representative sample of galaxies within voids. To obtain a precise characterization of the voids, they should be fully included in the survey and should contain at least 20 galaxies spread at various void-centric distances. Voids located near the edges of the SDSS footprint were eliminated because their centers and geometries could not be properly assessed. After a careful statistical characterisation of the remaining voids, a subsample of voids was selected that spans the largest ranges of effective radius, number of galaxies, and volume number density of galaxies. This defines a mother sample of around 3 000 galaxies. A subsample of the order of 200–300 galaxies is being observed with the PMAS instrument (Roth et al. 2005) on the 3.5m telescope of Calar Alto observatory.

2.2. CosmicFlows-3

In order to assess the dynamics of the voids in the CAVITY sample, we use the matter distribution implied by the peculiar galaxy velocities in the CosmicFlows-3 (CF3) catalog. The third release of the CosmicFlows catalog compiles about 18 000 measurements of galaxy distances and provides a corresponding cosmography on a three-dimensional grid in supergalactic coordinates, which is used in this article. The recently released fourth version of the CosmicFlows catalog (CF4) delivers about 56 000 galaxies and about 1 000 Type Ia supernovae distance measurements (Tully et al. 2023).

The combined measurements of galaxy luminosity distances and recessional velocities in the CF3 catalogue allows us to map the full matter overdensity field in the local Universe out to $z < 0.05$. The observational data are combined within an iterative forward modeling analysis (Graziani et al. 2019) within the Λ CDM paradigm of Planck Collaboration et al. (2016). This analysis entails a comprehensive incorporation of local over- and underdensities and their associated peculiar (or gravitational) velocity fields.

Assuming that the mass fluctuations $\delta_m(\mathbf{x}, t)$ reside in the linear regime, the full dark+luminous matter at position and time (\mathbf{x}, t) is obtained on the basis of the reconstructed full 3D matter peculiar velocity field \mathbf{v}_m by:

$$\nabla \cdot \mathbf{v}_m = -aHf(\Omega_m)\delta_m(\mathbf{x}, t), \quad (1)$$

in which a is the scale factor of the Universe, H is the Hubble expansion rate, Ω_m is the cosmological mass-density parameter, and $f(\Omega_m)$ is the (linear) structure growth rate (Peebles 1980). The growth rate $f(\Omega_m)$ depends on the cosmological parameter Ω_m used for the computation. The CF3 density field $\delta_m(\mathbf{x})$ is computed on a 256^3 grid of size $500 \text{ h}^{-1}\text{Mpc}$. This yields a resolution of about $2\text{h}^{-1}\text{Mpc}$ per voxel (A voxel is the smallest resolved volume in a 3D grid. Its size is the resolution of the grid.)

3. Void analysis

As we intend to compare the matter content of voids inferred from the galaxy redshift distribution to that computed from the peculiar velocity dynamics, we need to follow void-identification procedures that allow us to trace voids in the two corresponding situations. The first void-detection procedure

seeks to trace voids in the discrete spatial distribution of galaxies.

3.1. Void detection and identification in the SDSS galaxy redshift survey

The catalogue of cosmic voids extracted from the SDSS DR7 galaxy sample was identified with the VoidFinder procedure (El-Ad & Piran 1997; Hoyle & Vogeley 2002, 2004; Pan et al. 2012). In a first step, the algorithm classifies the galaxies of the sample into field and wall galaxies using the third nearest neighbour distance d_3 in relation to a threshold distance $d_{thr} = 6.3\text{h}^{-1}\text{Mpc}$. A field galaxy is a candidate for belonging to a void-like region ($d_3 > d_{thr}$), whereas a wall galaxy lies within a denser region, such as a filament or cluster ($d_3 < d_{thr}$). The wall galaxies are used to define the survey density grid. Starting from empty grid cells, empty spheres are grown until they can be defined by four boundary wall galaxies. The largest spheres are taken to be voids. The smaller spheres with more than 10 % overlap are merged with the larger voids. Once these mergers are complete, the void centers are taken to be the centers of mass of the empty spheres defining a void. An in-depth description of the procedure is given in Hoyle & Vogeley (2002) and the specific details of this DR7 sample are provided in Pan et al. (2012).

3.2. Void characterization and void parameters

The most prominent void properties are their size and density profiles.

3.2.1. Void density profiles

The major goal of our analysis is to compare the radial galaxy number density profile $\delta_g(r)$ and the corresponding radial mass-density profile $\delta_{m,v}^{CF3}(r)$ of each of the voids in our sample and to decipher whether or not there exists a relationship between the two. We seek to establish how far galaxies in and around the voids in our sample trace the underlying mass distribution inferred from the velocity field analysis in the CF3 catalog.

We computed the galaxy number density profile $\delta_g(r)$ of the seven voids of our sample using redshift survey positions of the galaxies residing within them (with equation 2). This profile is estimated by counting the number of SDSS galaxies in various shells of radii r_i/R_v around the center of each void. The profile computation involves 40 radial bins of width $\Delta r = 0.125 R_v$, ranging over the interval $r_i/R_v=0.0$ to 5.0. The number counts of galaxies in the radial bins around the void centers are normalized by the number counts of a random galaxy sample that follows the same angular coverage and radial selection function as the galaxy sample, as expressed formally in equation (2), in which the random sample consists of ten times more objects than the observed galaxy sample.

The resulting radial density profile estimate $\delta_g(r)$ is equal to the radial correlation function $\xi(r)$ around a single void center:

$$\delta_g(r) := \xi(r) = \frac{n_R D_{vg}(r)}{n_D R_{vg}(r)} - 1. \quad (2)$$

In the above expression, we follow the Davis-Peebles estimator of the correlation function (Davis & Peebles 1983). The number of galaxies around a void center at radius r is given by $D_{vg}(r)$, while the number of galaxies around a void center in the random galaxy sample is given by $R_{vg}(r)$. The ratio between the total

number of data sample galaxies n_D and that in the random sample n_R , n_R/n_D , constitutes the required normalization. Hence, in practice, the estimate of $\xi(r)$ is the galaxy number density contrast.

The radial mass-density profiles $\delta_{m,v}^{CF3}(r/R_v)$ of each void are determined from the mass-density field δ_m reconstruction from the CF3 survey. The mass-density field is represented on a 256^3 grid of $2h^{-1}\text{Mpc}$ voxels. The radially averaged mass-density profile $\delta_{m,v}^{CF3}(r_i/R_v)$ around voids measures the mean full matter (dark+luminous) density from the void center $r = 0$ to its outskirts $r/R_v > 1$.

In order to also include the environment of each individual void, the mass and galaxy number density profiles are computed from $r/R_v = 0, \dots, 5$. The profile measures the average matter density in radial shells of width Δr , including the voxels i with a radial distance in the range $r - \Delta r/2 < r_i < r + \Delta r/2$. The profile is determined from the grid-based density field $\delta_{m,i}^{CF3}$ as follows:

$$\delta_{m,v}^{CF3}(r/R_v) = \frac{1}{N_{\text{voxel}}} \sum_i \delta_{m,i}^{CF3}. \quad (3)$$

Hence, the void matter density profile computed from the CF3 density grid is the average density in radial bins of size $\Delta r = 5/40 = 0.125 R_v$, where N_{voxel} is the number of voxels found at a separation of r/R_v and $\delta_{m,i}^{CF3}$ is the value of the CF3 density field in the voxel i found at a separation of r_i/R_v .

The CF3 grid resolution is $2 h^{-1}\text{Mpc}$, while the CAVITY voids—which are identified using a galaxy number density field—span an interval of mean effective radii of $15 h^{-1}\text{Mpc} < R_v < 25 h^{-1}\text{Mpc}$.

4. Voids and their large-scale environment

In order to be able to interpret the results we obtain for the relation between the distribution of galaxies and the total mass in and around voids, we carried out a visual inspection. This enables a direct study of the large-scale environment of the void sample.

Figure 1 is an interactive plot that the reader can use to better grasp the locations of the seven voids in comparison with the matter density contrast distribution as computed using the CosmicFlows-3 catalog. Figure 2 shows the supergalactic SGY–SGZ plane orientation with a thickness of $-2000 < SGX < 2000$ km/s. This plane helps to visualize how voids 355 and 738 belong to the same underdense region and may well be counted as a single "Hercules void". Two voids are located near the backside infall of Coma supercluster, namely 487 and 727. Their central overdensity as computed from CF3 is directly linked to this large-scale structure.

4.1. Hercules supercluster and void 355

Figure 3 shows the region around the Hercules supercluster. Three of the voids of our sample are located around this large-scale mass concentration; namely voids 355 and 738 on the nearer side, and void 142 on the far side of the supercluster. Of importance for our purpose are the locations of these three voids: while all are near the Hercules supercluster, they are more precisely located in the underdense interior of the surrounding mass distribution. An exciting goal of the CosmicFlows peculiar velocity project is to fully dynamically determine the total mass of the Hercules supercluster (?).

Figure 4 presents a zoom onto the cosmic V-web (Pomarède et al. 2017) reconstruction, which was computed using the shear tensor of the peculiar velocity field in and around void 355. The color code of the target galaxies is as follows: black, blue, yellow, and red galaxies are those that reside in a V-web environment classified as empty, sheet, filament, or node, respectively. Isosurfaces colored light gray to dark gray correspond to full matter contrast levels of $\delta_m = -0.3, -0.7, \text{ and } -1.1$, respectively. We can clearly see the galaxies in black (V-Web type: "void") in the center of the void, the blue ones ("sheet") on the periphery, and some yellow ("filament") on the side of Hercules/Great Wall, and there are no galaxies in red (classified as "knot"). The CF3 V-web reveals the very coherent dynamical pattern of this void 355, where both galaxy and matter-density profiles are in perfect agreement (see Fig. 4 and Section 5). Also, Fig. 4 clearly reveals the evacuation by means of the pattern of velocity vectors (black). These arrows depict the local flow with respect to the center of the underdensity. The interactive version of the figure is made available at [V-web environment of Void 355].

4.2. Coma supercluster and void surroundings

The Coma-Leo complex in the bottom right-hand corner of the mass-density map in Figure 2 is surrounded by several CAVITY voids. At least three of these, voids 482, 487, and 727, are lying in or touching the overdense outskirts of the complex. We should not be surprised to find that the galaxy density and the mass density inferred from the CF3 peculiar velocity field may substantially differ (see 5). Below, we argue that this may be a direct manifestation of the impact of the void environment on the dynamics and evolution of voids.

4.3. Void sociology and hierarchical void evolution

Visual appraisal of the void configurations in our study reveals that they provide an interesting and representative mixture of voids in different large-scale environments. Some are more isolated or remote with respect to overdense mass concentrations (e.g., voids 405 and 738), while others reside in or near the outskirts of nearby mass concentrations. Voids 355 and 142 are close to the Hercules supercluster, and voids 482, 487, and 727 are in the outskirts of the Coma region, with 439 partly embedded inside the Coma supercluster. This means that the sample can be used to probe the effects of nearby mass concentrations on the dynamics of voids.

Although the structure and evolution of voids is often discussed in terms of singular void configurations (see Appendix A), recognizing that they are not isolated objects is of utmost importance for properly understanding them. Given the relatively mild level of their density deficit, namely $|\delta| < 1$, external mass concentrations remain a major influence in the force inventory of voids (see Sheth & van de Weygaert 2004; van de Weygaert 2016). Moreover, when we consider the population of underdensities in the mass distribution, we find that the canonical deep under-dense near-spherical void regions that expand in each direction represent a smaller fraction of the void population. Most underdensities may expand along one or two dimensions, but contract along the other directions (Sheth & van de Weygaert 2004; Lavaux & Wandelt 2010). These voids tend to remain smaller, and may even collapse because of the surrounding over-densities. This latter process is called *void-in-cloud* (Sheth & van de Weygaert 2004).

Voids in the CAVITY Survey versus CF3 reconstruction

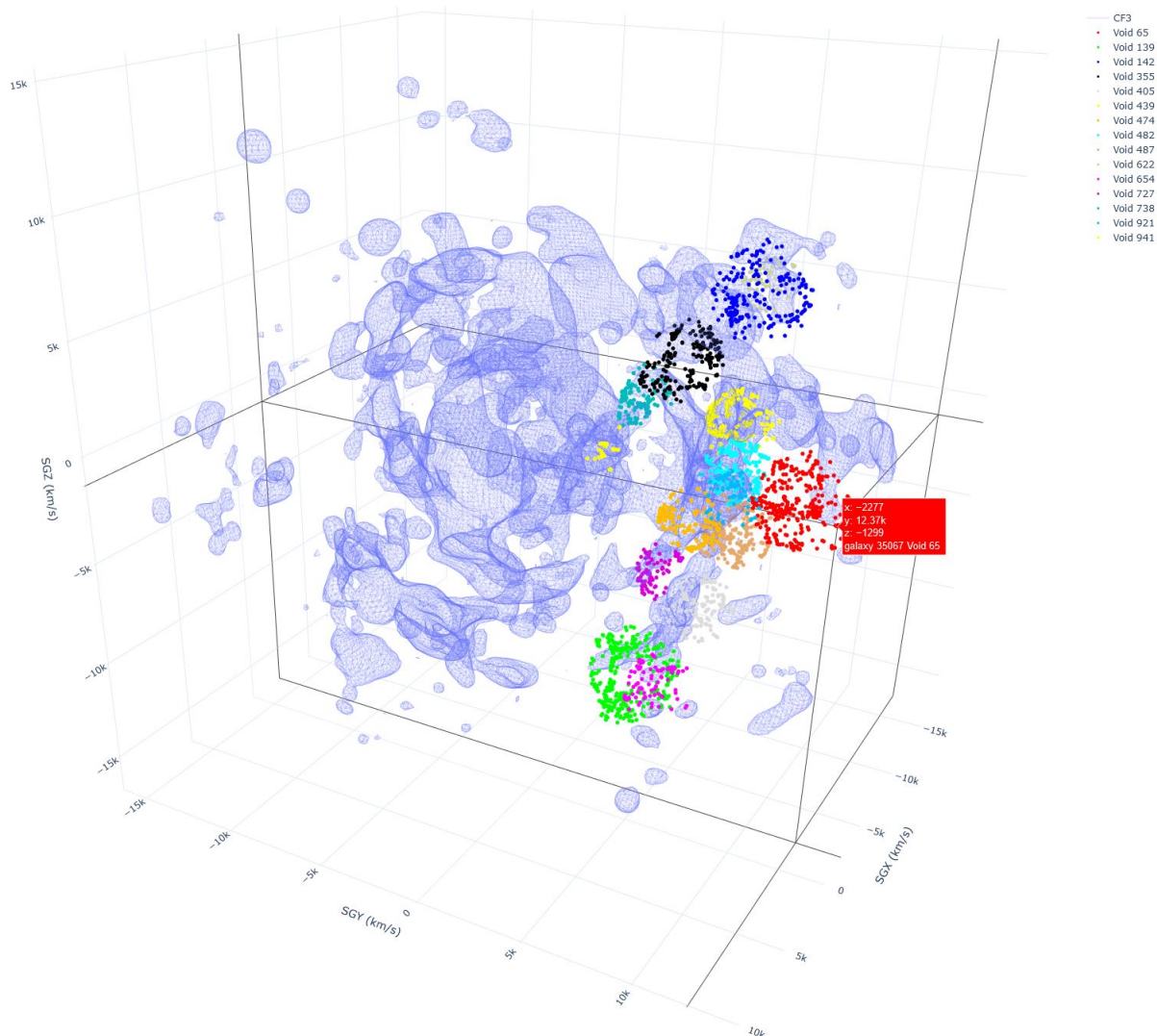


Fig. 1: Interactive 3D visualization of the distribution of nearby voids [Start Interaction]. The positions of the CAVITY survey target galaxies are given by markers colored according to their void membership as indicated in the column displayed on the right-hand side. In the online version, hovering over the galaxy markers reveals the galaxy positions, identifiers, and void memberships. The wireframe polygon is a high-density ($\delta_m = 1.3$) isosurface of the reconstructed CosmicFlows-3 overdensity field. Also in the online version, the user can rotate, pan, and zoom in and out using the mouse. Single-click or double-click on the elements listed on the right-hand side column hides them or singles them out from the scene.

4.3.1. Hierarchical void evolution

On the basis of the dynamics and location, we may recognize two principal processes of void evolution (Sheth & van de Weygaert 2004). *Void-in-void* refers to the process whereby expanding voids merge into even larger voids, resembling the fate of soap bubbles in a bath (see e.g., Dubinski et al. 1993). For voids in or near high-density regions that dominate their dynamical evolution, the *void-in-cloud* process refers to the disappearance of voids because of the gravitational contraction and collapse induced by the environment.

The physical context is such that there is a hierarchy of voids, with the velocity field dominated by large expanding voids, interior to which are found smaller, often elongated voids, in particular near the edges of the large expanding voids (see Fig. 11 of van de Weygaert (2016)). These smaller voids may contract

along one or two dimensions, or even fully collapse. Also important is the fact that many of these voids are not spherical at all, but become substantially deformed by dominant tidal influences of the surrounding mass concentrations. This process may even involve fully collapsing voids entirely embedded in overdense structures.

Hierarchical void evolution leads to a situation in which it may not be straightforward to relate velocity flow and density in and around voids, as much of the (filtered) flow field includes the dynamical influence of the nearby high-density regions. A detailed study and analysis of the corresponding properties of the hierarchical embedding of void flows, particular in terms of the velocity divergence, is presented by Aragon-Calvo & Szalay (2013) and also see Aragon-Calvo et al. (2010).

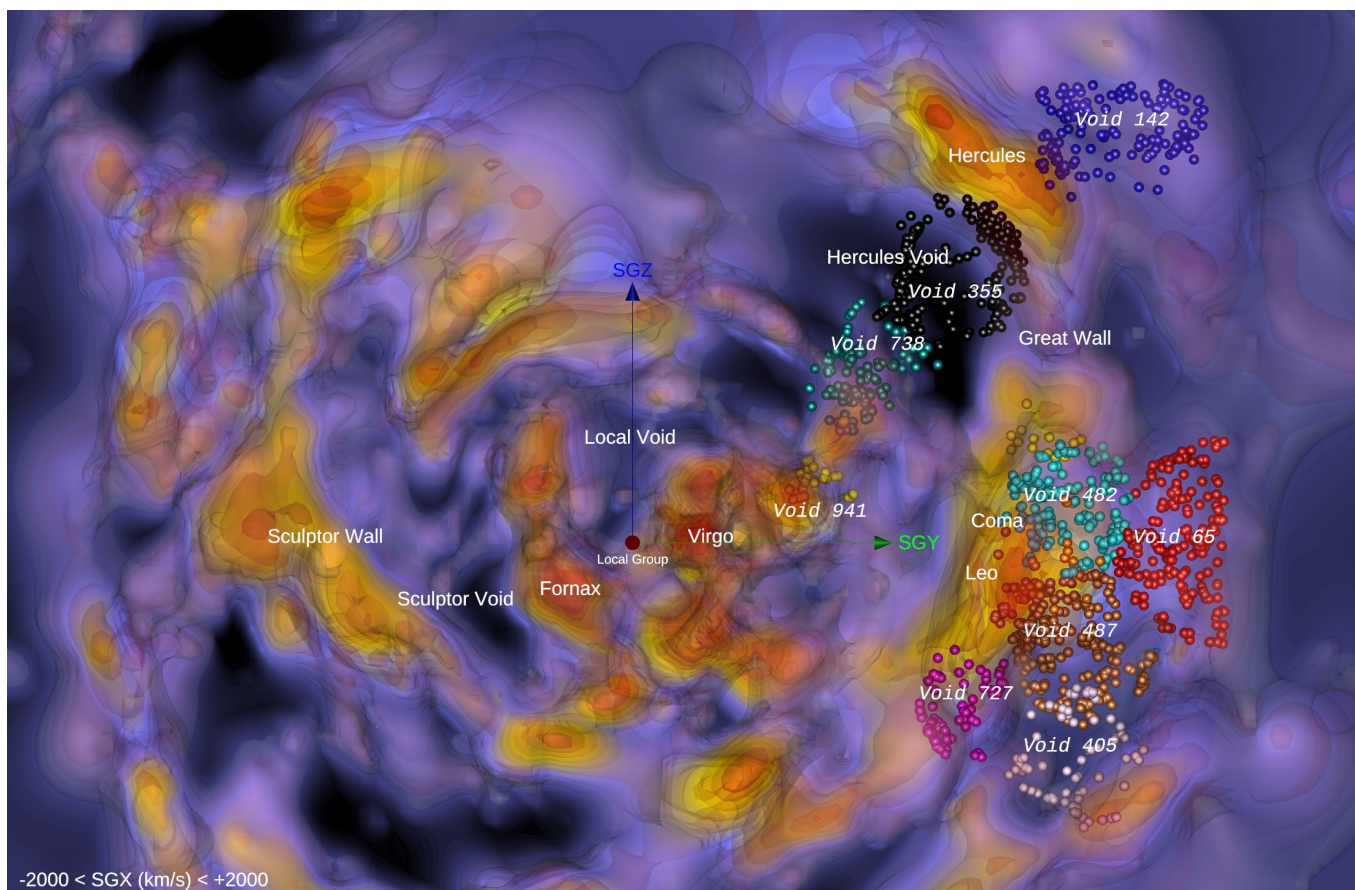


Fig. 2: Map of a sample void against the reconstructed CosmicFlows-3 density field. Map of galaxy and mass distribution within a slice $-2000 < SGX < 2000$ km/s. Galaxy markers are colored according to their void membership. Scale and orientation are given by the 5000 km/s long green (SGY) and blue (SGZ) arrows emanating from our position, associated with the cardinal axes of the Supergalactic Coordinate System.

4.4. Void environment and dynamical impact

Following the observation of diverse void environments in our sample, and the implications for their dynamical evolution and fate, a quantitative and statistical analysis of the environmental imprint is presented in the following section. The results show that the visual inspection of the position of voids compared to the well-known large-scale structures in the local Universe is indeed confirmed quantitatively. The identification of voids in galaxy-redshift surveys appears to lead to the inclusion of voids that partake in the *void-in-cloud* process (see sect. 5), that is, voids that are contracting—along one, two, or three directions—because of the over-dense surroundings. In simulations, these are usually the small voids near the filamentary and wall-like boundaries of large voids (Sheth & van de Weygaert 2004). Early indications of this were found in the SDSS survey by the redshift space correlation function analysis by Paz et al. (2013). In other words, our analysis indicates that this is the state of some of the CAVITY voids.

5. Emptiness of voids: Results

In this section, we compare the δ_g values from galaxy redshift counts to the CF3 reconstruction δ_m contrast field on the basis of the galaxy and mass-density profiles of the seven voids included in our sample. Figure 4 shows the galaxy counts around the seven

voids (left panels) together with the mass and galaxy number density profiles (right panels).

The left panels of fig. 4 show the number of galaxies in the galaxy samples—namely SDSS, SDSS void galaxies only, and CosmicFlows third and fourth editions—as a function of radial distance (in normalized units) r/R_v . For six voids, we see the expected pattern of a steeply increasing number of galaxies as a function of radius around a near-empty void interior. Only void 941, which is found near the outskirts of the Virgo cluster (see Fig. 2), displays a slightly different behavior. Many galaxies are found within half its effective radius R_v .

The galaxy number-density profiles (purple dashed lines) and mass-density profiles (solid blue lines) reveal a different story. The profiles in all seven right-hand panels agree on their tendency towards the global mean density value of $\delta_m=0$ at $r/R_v > 3$ (the average of the density field over all dimensions in the full CF3 grid gives a value of a mean $\delta_m = 0.005$). This implies that all void configurations consist of a central void surrounded by over-dense structures within $1 < r/R_v < 3$. Most importantly, in at least half of the sample of voids, there is a strong difference between the computed galaxy number-density profile and the mass-density profile inferred from the peculiar velocity field.

While the galaxy number-density profiles for almost all the voids of our sample display the well-known “bucket-shaped” inner profile, the CF3-implied mass profiles show a different behavior. For half of our small sample of seven voids, there

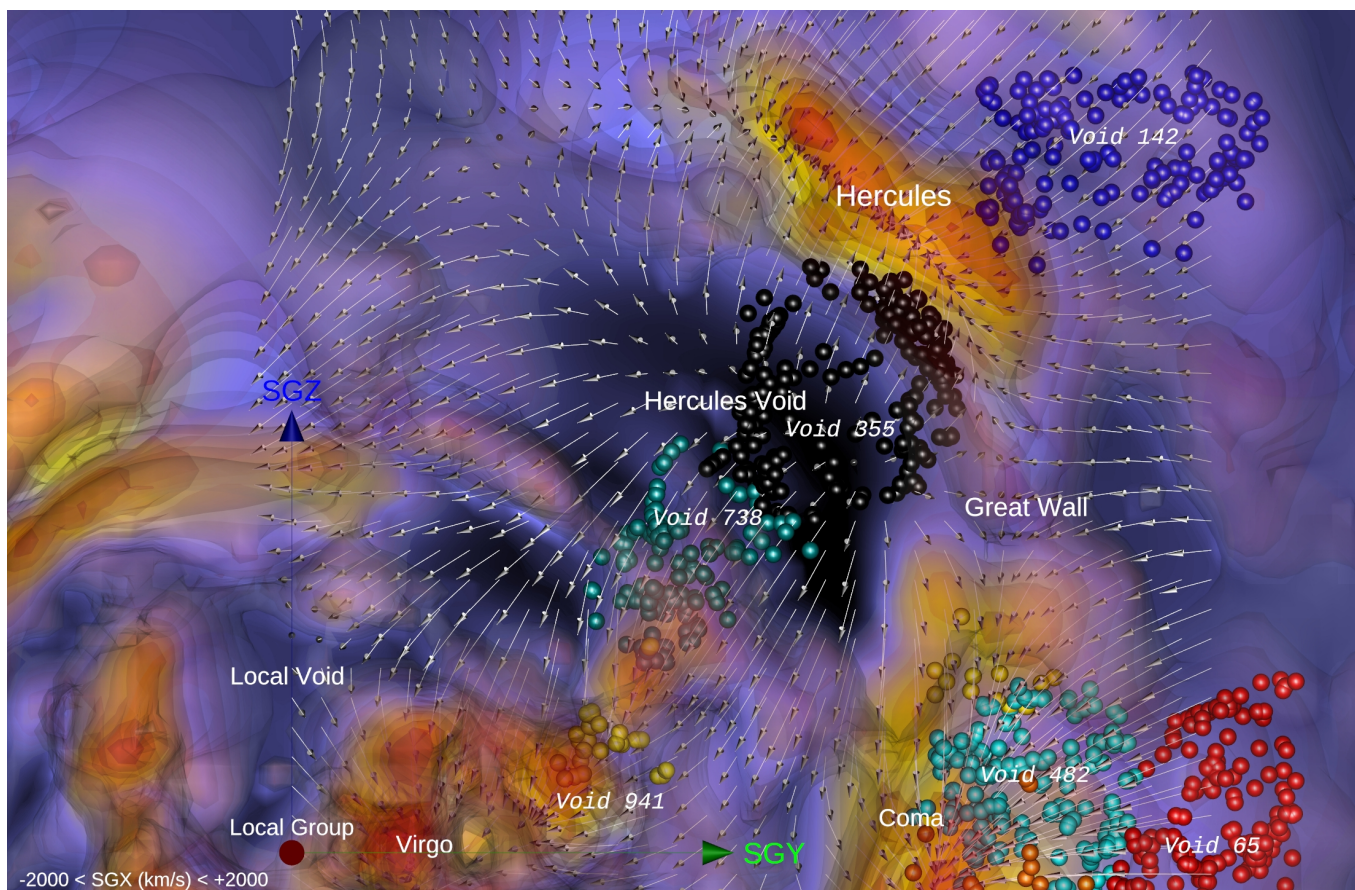


Fig. 3: Focus on the Hercules region. The positions of galaxies are plotted against the reconstructed CosmicFlows-3 density contrast and velocity field, within a slice $-2000 < SGX < 2000$ km/s. Galaxy markers are given distinct colors as a function of their void membership. Scale and orientation are given by the 5000 km/s long green (SGY) and blue (SGZ) arrows emanating from our position, associated with the cardinal axes of the Supergalactic Coordinate System. The map shows that the galaxies within Void 355 and Void 738 are subject to the evacuation of matter from the Hercules Void, as mapped by the divergent flow at this location. Voids 355 and 738 belong to the same underdense region and may well be counted as a single "Hercules void".

is strong disagreement in the void emptiness when computed from galaxy counts (empty) and from peculiar velocity dynamics (overdensity near the center). Only in the case of void 355 do we find perfect agreement between galaxy number-density and mass-density profiles. This may relate to the fact that void 355 is a relatively large and well-defined void of which a significant part is located near the center of the Hercules void-mass underdensity. On the other hand, in the case of three or even four voids, we find implied mass overdensities near the center. In summary, the blue solid lines in fig. 4 show that the CF3-reconstructed matter profiles (computed using equation 3) do not systematically display underdense regions near the void centers. As discussed in section 4, some of these voids have centers located in overdense regions in CF3.

When analyzing and interpreting these results, it is important to take into account the differences between the probes used to trace the CF3 and the CAVITY probes. The detected voids in different galaxy samples are sensitively dependent on the number density and nature of the galaxy population in those samples (Peebles 2001; Gottlöber et al. 2003; Tinker et al. 2006, see). It is self-evident that voids in more diluted galaxy samples will be larger on average, as these samples lack the spatial resolution to resolve the smaller voids. A more profound influence is the fact that the spatial clustering of galaxies is also sensitively dependent on the galaxies in the sample. Brighter and heavier galaxies

are more strongly clustered, and there will therefore be larger "cavities" in their spatial distribution. A recent study found that the void population in different galaxy populations is indeed dependent on higher-order clustering properties of the galaxy population, in excess of its two-point clustering properties (Bermejo et al. 2022). These authors found proof of a strongly systematic dependence of the void population on the topological characteristics of the spatial galaxy distribution. In other words, voids detected in different galaxy populations are strongly affected by a topological bias.

Evidence that this subtle galaxy bias affects the void population and inferred void-density profiles was pointed out in the analysis of voids in the SDSS galaxy survey by Ricciardelli et al. (2013). These authors found that differences in void probes lead to systematic differences between void-density profiles based on galaxy counts and voids extracted from the density distribution in simulations. This may certainly be a factor of relevance in the comparison between the CAVITY and CF3 voids in the present study. However, while this bias can undoubtedly play a role, it cannot explain our results since the levels of anti-bias required would be unrealistic (Braun et al. 1988).

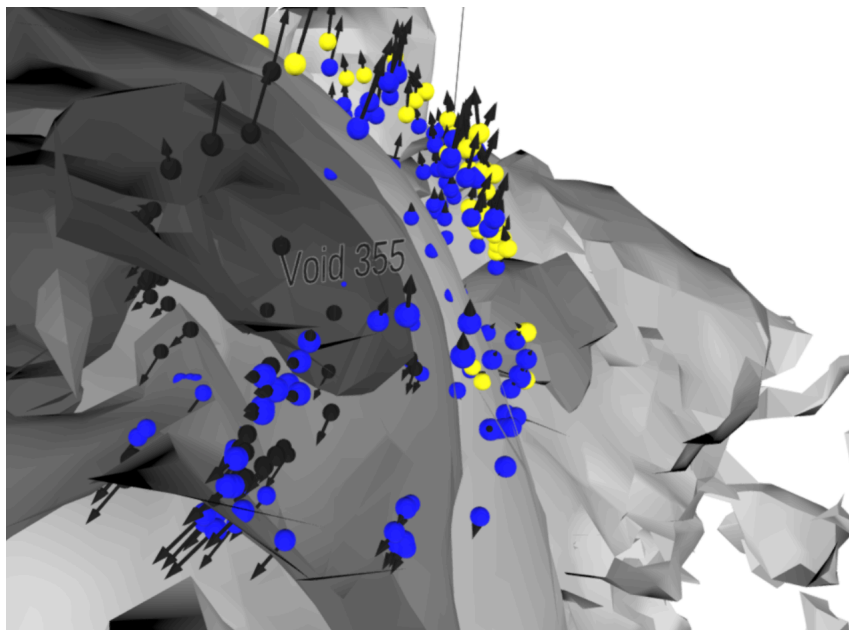


Fig. 4: V-web environment as computed using the shear tensor of the CF3 peculiar velocity field for void 355. The color code of the target galaxies is as follows: black, blue, yellow, and red identify galaxies in a V-web environment classified as empty, sheet, filament, or node, respectively. Isosurfaces in light gray to dark gray correspond to full-matter contrast levels of $\delta_m = -0.3, -0.7,$ and -1.1 respectively. One can clearly see the evacuation of the local flow (the speed from the center of the vacuum was subtracted). The interactive version of the figure is available here: [V-web environment of Void 355].

6. Discussion and conclusions

In the presented analysis, we compare the galaxy distribution in and around a small sample of seven voids from the CAVITY void galaxy survey with the dynamically inferred mass distribution in and around voids. The latter distribution is based on the mass reconstruction from the velocity flow field measured using the Cosmicflows-3 catalog. The comparison between the mass and galaxy distributions around these voids, in conjunction with the map of the large-scale mass distribution and features in and around these voids in the Local Universe, enables us to assess the impact of environment on the dynamics and hierarchical evolution of the void population. The results of this comparison demonstrate the reality and importance of the void-in-cloud process in the buildup of the web-like matter distribution in the Universe. Our findings also reveal the importance of distinguishing these voids from the dominant fully expanding voids—the result of the void-in-void merging process—when we seek to study the role of voids in a cosmological setting (e.g., van de Weygaert 2016; Pisani et al. 2019) or when assessing their influence on galaxy formation and the galaxy star formation history (see Goldberg & Vogeley 2004; Lackner et al. 2012, for theoretical treatments).

The sample of seven CAVITY voids was identified with a classical void finder from the SDSS redshift survey. Using a similar algorithm we confirm that local voids are empty of galaxies near their center and roughly up to their effective radius. However, a different picture emerges when studying the velocity field in and around these voids. When assessing the dynamics of the

void regions, and computing the matter content from the measured CF3 velocity flows, in half of the cases, we find that on the corresponding scale of the velocity flows these void regions are not underdense.

There are several reasons why the mass and galaxy distribution around the sample voids may be different. One factor is that of galaxy bias, with the galaxy population not entirely reflecting the underlying mass distribution. While we do not exclude this factor, we find that the strong levels of anti-bias that would be needed to explain our results are unrealistic (Peebles 2001; Gottlöber et al. 2003; Tinker et al. 2006; Ricciardelli et al. 2013; Bermejo et al. 2022). We believe that the overriding reason for the difference is to be found in the location of the voids with respect to their surroundings. Several voids of the sample are located in or are identified with large underdensities in the mass distribution. The most interesting ones, slightly more than half of the sample, are found at the outer regions of the Coma-Leo and Virgo mass supercluster complexes.

A major part of the explanation for the difference between the galaxy distribution in and around these voids and the inferred large-scale mass distribution is the dynamical impact of the void environment. The void regions affiliated with large underdensities in the CF3 map of the Local Universe partake in the overall expansion of the region. The divergent velocity flow translates into a corresponding void mass-density profile. This latter is a typical manifestation of the so-called void-in-void configuration that goes along with the hierarchical buildup of the void population (Sheth & van de Weygaert 2004).

However, in our void sample, we find that the majority of CAVITY voids most likely belong to the class of voids that are not expanding in three dimensions, and may even contract along one or two dimensions. These void-in-cloud voids (Sheth & van de Weygaert 2004) represent the majority of the underdense regions in the mass distribution, and in the hierarchical buildup of structure are often found at the boundaries of large voids and surrounding overdense filaments and walls. The flow in and around these voids is largely dominated by the dynamical—tidal— influence of the nearby overdense filaments and walls. This translates into an anisotropic and in some cases even fully collapsing flow field in and around the void, which explains the difference between the galaxy underdensity and the implied mass distribution, which includes the contribution from the surrounding overdense large-scale structure. Hence, while on the large linear scales we find the overdensity as it takes into account the large-scale surroundings, on smaller scales we would recover the underdensity that is also seen in the galaxy distribution. This explains why the galaxy counts may hint at a local cavity, while the CF3 velocity flow would suggest otherwise.

Within the context of the hierarchically evolving void population, and the role of the surroundings in the evolution of voids, we may also find the merging of voids with overdense walls or filaments. A recent theoretical study (Vallés-Pérez et al. 2021) found that $\sim 10\%$ of the mass in voids at $z = 0$ may be accreted from overdense regions, with this value even reaching beyond 35% for a significant fraction of voids.

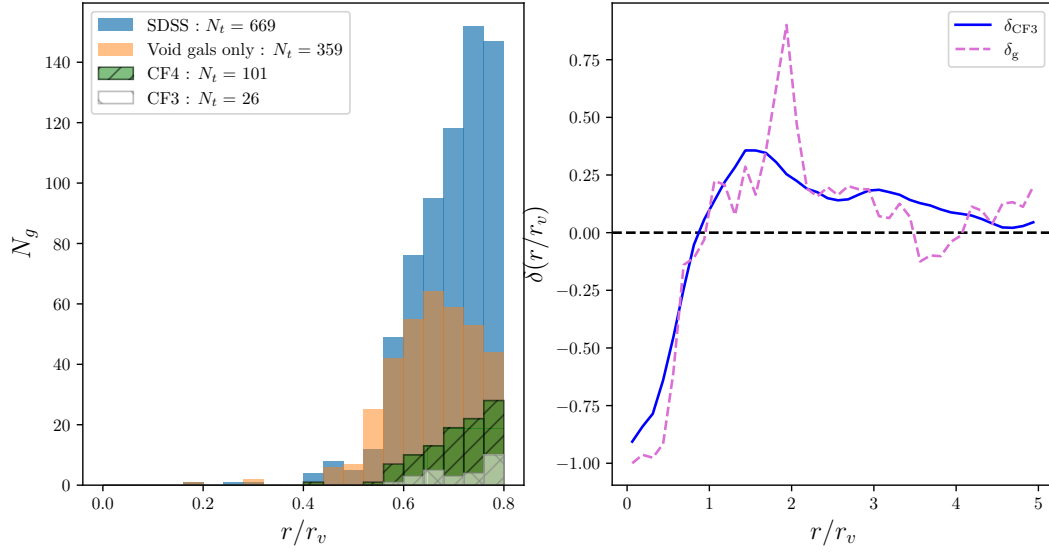
While the present analysis of a limited void sample demonstrates the potential for studying voids in relation to their large-scale environment, we expect exciting and statistically representative results for the Local Universe void population from the recently released CosmicFlows-4 dataset of galaxy distances, which includes the entire SDSS volume (Courtois et al. 2023).

Acknowledgements. HC is grateful to the Institut Universitaire de France for its support. HC, MA, DG acknowledge support from the CNES. RvdW is grateful to Miguel Aragon-Calvo, Job Feldbrugge, Roi Kugul, Bernard Jones, Georg Wilding and Raul Bermejo on numerous discussions on the nature of voids and the role of topological bias. E.F. is grateful to the Spanish 'Ministerio de Ciencia e Innovación and from the European Regional Development Fund (FEDER) via grants PID2020-224414GB-I00 and PID2020-113689GB-I00, and from the 'Junta de Andalucía' (Spain) local government through the FQM108 and A-FQM-510-UGR20 projects. L.G. acknowledges financial support from the Spanish Ministerio de Ciencia e Innovación (MCIN), the Agencia Estatal de Investigación (AEI) 10.13039/501100011033, and the European Social Fund (ESF) "Investing in your future" under the 2019 Ramón y Cajal program RYC2019-027683-I and the PID2020-115253GA-I00 HOSTFLOWS project, from Centro Superior de Investigaciones Científicas (CSIC) under the PIE project 20215AT016, and the program Unidad de Excelencia María de Maeztu CEX2020-001058-M. RGB acknowledges financial support from the grants CEX2021-001131-S funded by MCIN/AEI/10.13039/501100011033 and PID2019-109067-GB-I00. KK gratefully acknowledges funding from the German Research Foundation (DFG) in the form of an Emmy Noether Research Group (grant number KR4598/2-1, PI Kreckel). SP and VQ acknowledge support by the Agencia Estatal de Investigación Española (AEI; grant PID2019-107427GB-C33), by the Ministerio de Ciencia e Innovación (MCIN) within the Plan de Recuperación, Transformación y Resiliencia del Gobierno de España through the project ASFAE/2022/001, with funding from European Union NextGenerationEU (PRTR-C17.11), and by the Generalitat Valenciana (grant PROMETEO/2019/071). JR acknowledges support from the State Research Agency (AEI-MCINN) of the Spanish Ministry of Science and Innovation under the grant "The structure and evolution of galaxies and their central regions" with reference PID2019-105602GB-I00/10.13039/501100011033, funding granted for his Margarita Salas Fellowship by the Ministry of Universities granted by Order UNI/551/2021 of May 26, as well as funding by the European Union-Next Generation EU Funds. MSP acknowledges support from the Spanish Ministry of Science and Innovation through project AYA2017-88007-C3-2-P.

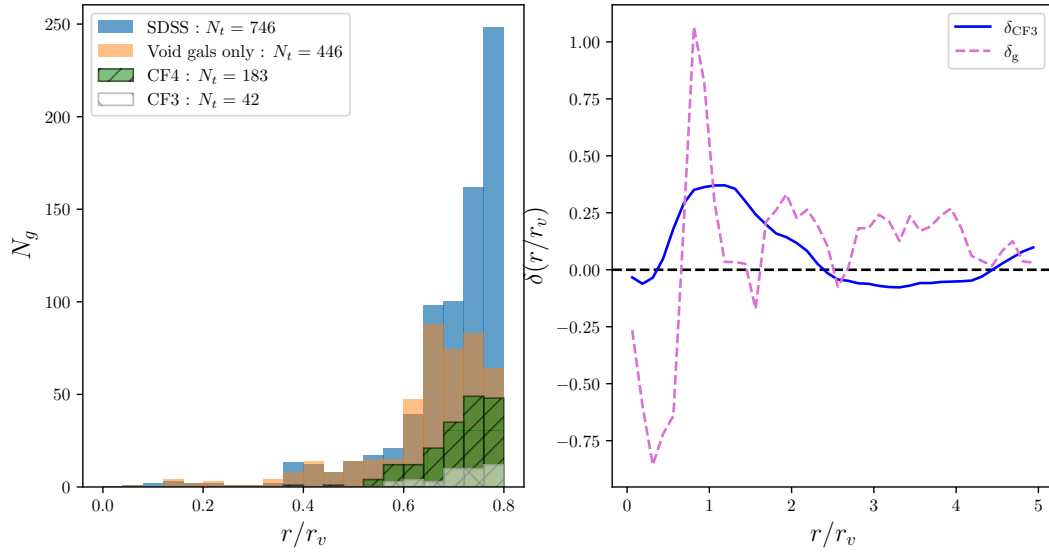
References

- Aragon-Calvo, M. A. & Szalay, A. S. 2013, *MNRAS*, 428, 3409
- Aragon-Calvo, M. A., van de Weygaert, R., Araya-Melo, P. A., Platen, E., & Szalay, A. S. 2010, *MNRAS*, 404, L89
- Bermejo, R., Wilding, G., van de Weygaert, R., et al. 2022, arXiv e-prints, arXiv:2206.14655
- Bertschinger, E. 1985, *ApJ*, 295, 1
- Beygu, B., Kreckel, K., van der Hulst, J. M., et al. 2016, *MNRAS*, 458, 394
- Beygu, B., Peletier, R. F., van der Hulst, J. M., et al. 2017, *MNRAS*, 464, 666
- Blumenthal, G. R., da Costa, L. N., Goldwirth, D. S., Lecar, M., & Piran, T. 1992, *ApJ*, 388, 234
- Bond, J., Kofman, L., & Pogosyan, D. 1996, *Nature*, 380, 603
- Borzyszkowski, M., Porciani, C., Romano-Díaz, E., & Galardi, E. 2017, *MNRAS*, 469, 594
- Bos, E. G. P., van de Weygaert, R., Dolag, K., & Pettorino, V. 2012, *MNRAS*, 426, 440
- Braun, E., Dekel, A., & Shapiro, P. R. 1988, *ApJ*, 328, 34
- Cai, Y.-C., Padilla, N., & Li, B. 2015, *MNRAS*, 451, 1036
- Cautun, M., Cai, Y.-C., & Frenk, C. S. 2016, *MNRAS*, 457, 2540
- Cautun, M., van de Weygaert, R., Jones, B. J. T., & Frenk, C. S. 2014, *MNRAS*, 441, 2923
- Courtois, H. M., Dupuy, A., Guinet, D., et al. 2023, *A&A*, 670, L15
- Courtois, H. M., Hoffman, Y., Tully, R. B., & Gottlöber, S. 2012, *ApJ*, 744, 43
- Davis, M. & Peebles, P. J. E. 1983, *ApJ*, 267, 465
- de Lapparent, V., Geller, M. J., & Huchra, J. P. 1986, *ApJ*, 302, L1
- Domínguez-Gómez, J., Lisenfeld, U., Pérez, I., et al. 2022, *A&A*, 658, A124
- Dubinski, J., da Costa, L. N., Goldwirth, D. S., Lecar, M., & Piran, T. 1993, *ApJ*, 410, 458
- El-Ad, H. & Piran, T. 1997, *ApJ*, 491, 421
- Ganeshiah Veena, P., Cautun, M., Tempel, E., van de Weygaert, R., & Frenk, C. S. 2019, *MNRAS*, 487, 1607
- Goh, T., Primack, J., Lee, C. T., et al. 2019, *MNRAS*, 483, 2101
- Goldberg, D. M. & Vogeley, M. S. 2004, *ApJ*, 605, 1
- Gottlöber, S., Lokas, E. L., Klypin, A., & Hoffman, Y. 2003, *MNRAS*, 344, 715
- Graziani, R., Courtois, H. M., Lavaux, G., et al. 2019, *MNRAS*, 488, 5438
- Hahn, O., Porciani, C., Carollo, C. M., & Dekel, A. 2007, *MNRAS*, 375, 489
- Hamaus, N., Pisani, A., Sutter, P. M., et al. 2016, *Phys. Rev. Lett.*, 117, 091302
- Hamaus, N., Sutter, P. M., & Wandelt, B. D. 2014, *Phys. Rev. Lett.*, 112, 251302
- Hellwing, W. A., Cautun, M., van de Weygaert, R., & Jones, B. T. 2021, *Phys. Rev. D*, 103, 063517
- Hoyle, F. & Vogeley, M. S. 2002, *ApJ*, 566, 641
- Hoyle, F. & Vogeley, M. S. 2004, *ApJ*, 607, 751
- Huchra, J. P., Macri, L. M., Masters, K. L., et al. 2012, *ApJS*, 199, 26
- Icke, V. 1984, *MNRAS*, 206, 1P
- Kirshner, R. P., Oemler, A., J., Schechter, P. L., & Shtetman, S. A. 1981, *ApJ*, 248, L57
- Kreckel, K., Platen, E., Aragón-Calvo, M. A., et al. 2012, *AJ*, 144, 16
- Kreckel, K., Platen, E., Aragón-Calvo, M. A., et al. 2011, *AJ*, 141, 4
- Lackner, C. N., Cen, R., Ostriker, J. P., & Joung, M. R. 2012, *MNRAS*, 425, 641
- Lavaux, G. & Wandelt, B. D. 2010, *MNRAS*, 403, 1392
- Lavaux, G. & Wandelt, B. D. 2012, *ApJ*, 754, 109
- Pan, D. C., Vogeley, M. S., Hoyle, F., Choi, Y.-Y., & Park, C. 2012, *MNRAS*, 421, 926
- Paranjape, A., Hahn, O., & Sheth, R. K. 2018, *MNRAS*, 476, 3631
- Park, D. & Lee, J. 2007, *Phys. Rev. Lett.*, 98, 081301
- Paz, D., Lares, M., Ceccarelli, L., Padilla, N., & Lambas, D. G. 2013, *MNRAS*, 436, 3480
- Peebles, P. J. E. 1980, *The large-scale structure of the universe*
- Peebles, P. J. E. 2001, *ApJ*, 557, 495
- Pérez, I. & al. 2023 [in preparation]
- Perico, E. L. D., Voivodic, R., Lima, M., & Mota, D. F. 2019, *A&A*, 632, A52
- Pisani, A., Massara, E., Spergel, D. N., et al. 2019, *BAAS*, 51, 40
- Pisani, A., Sutter, P. M., Hamaus, N., et al. 2015, *Phys. Rev. D*, 92, 083531
- Planck Collaboration, Ade, P. A. R., Aghanim, N., et al. 2016, *A&A*, 594, A13
- Platen, E., van de Weygaert, R., & Jones, B. J. T. 2007, *MNRAS*, 380, 551
- Pomarède, D., Hoffman, Y., Courtois, H. M., & Tully, R. B. 2017, *ApJ*, 845, 55
- Ricciardelli, E., Quilis, V., & Planelles, S. 2013, *MNRAS*, 434, 1192
- Rojas, R. R., Vogeley, M. S., Hoyle, F., & Brinkmann, J. 2004, *ApJ*, 617, 50
- Rojas, R. R., Vogeley, M. S., Hoyle, F., & Brinkmann, J. 2005, *ApJ*, 624, 571
- Roth, M. M., Kelz, A., Fechner, T., et al. 2005, *PASP*, 117, 620
- Sheth, R. K. & van de Weygaert, R. 2004, *MNRAS*, 350, 517
- Tinker, J. L., Weinberg, D. H., & Warren, M. S. 2006, *ApJ*, 647, 737
- Tully, R. B., Courtois, H., Hoffman, Y., & Pomarède, D. 2014, *Nature*, 513, 71
- Tully, R. B., Courtois, H. M., & Sorce, J. G. 2016, *AJ*, 152, 50
- Tully, R. B., Kourkchi, E., Courtois, H. M., et al. 2023, *ApJ*, 944, 94
- Vallés-Pérez, D., Quilis, V., & Planelles, S. 2021, *ApJ*, 920, L2
- van de Weygaert, R. 2016, in *The Zeldovich Universe: Genesis and Growth of the Cosmic Web*, ed. R. van de Weygaert, S. Shandarin, E. Saar, & J. Einasto, Vol. 308, 493–523
- van de Weygaert, R. & Babul, A. 1994, *ApJ*, 425, L59
- van de Weygaert, R. & Platen, E. 2011, in *International Journal of Modern Physics Conference Series*, Vol. 1, International Journal of Modern Physics Conference Series, 41–66
- van de Weygaert, R. & van Kampen, E. 1993, *MNRAS*, 263, 481
- Verza, G., Carbone, C., & Renzi, A. 2022, *ApJ*, 940, L16
- Yan, H., Fan, Z., & White, S. D. M. 2013, *MNRAS*, 430, 3432

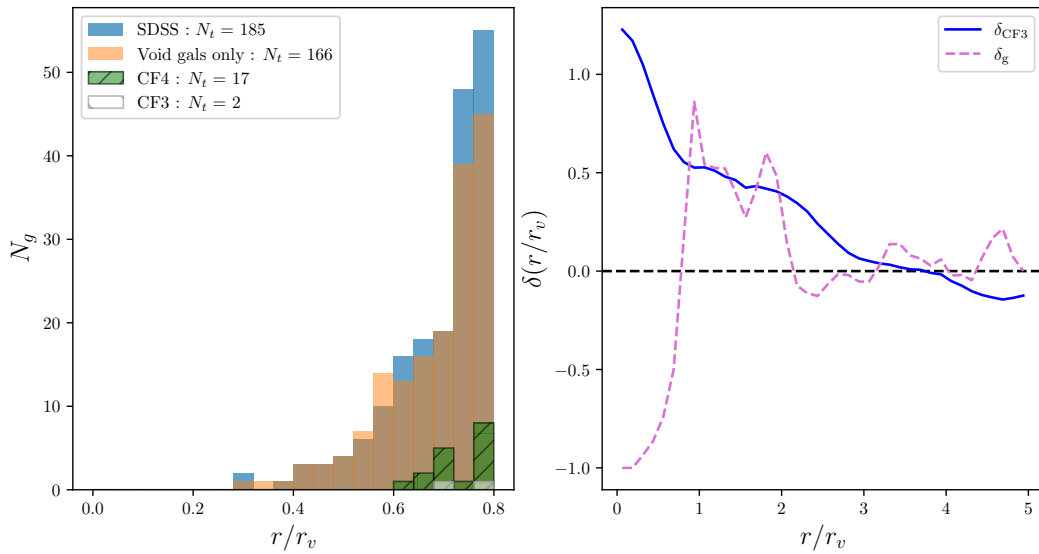
Void 355



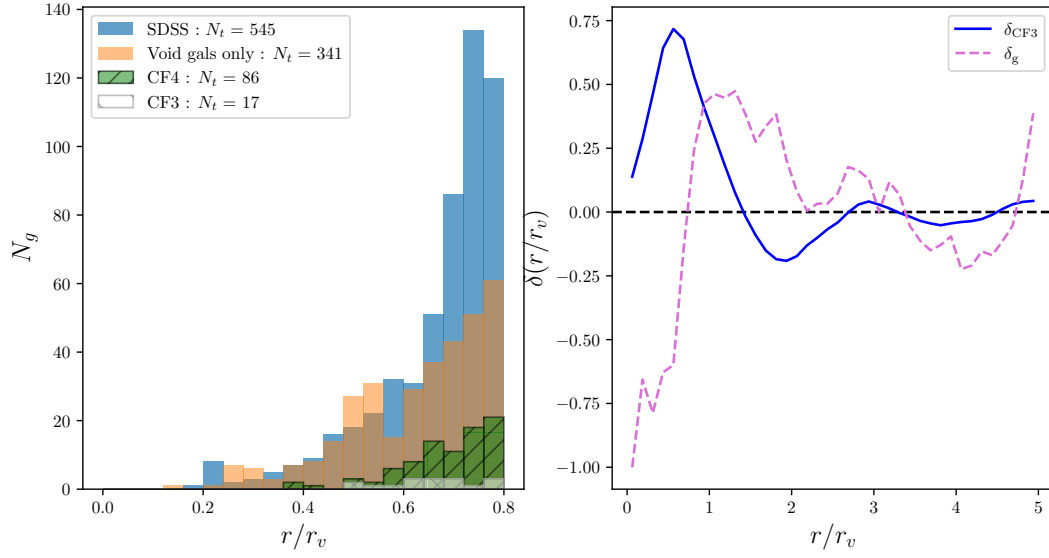
Void 439



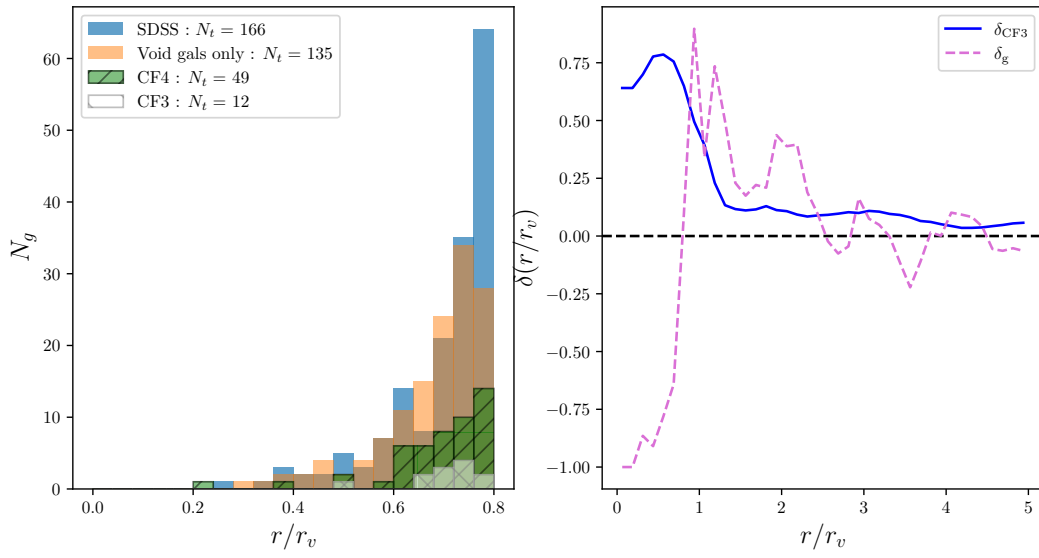
Void 474



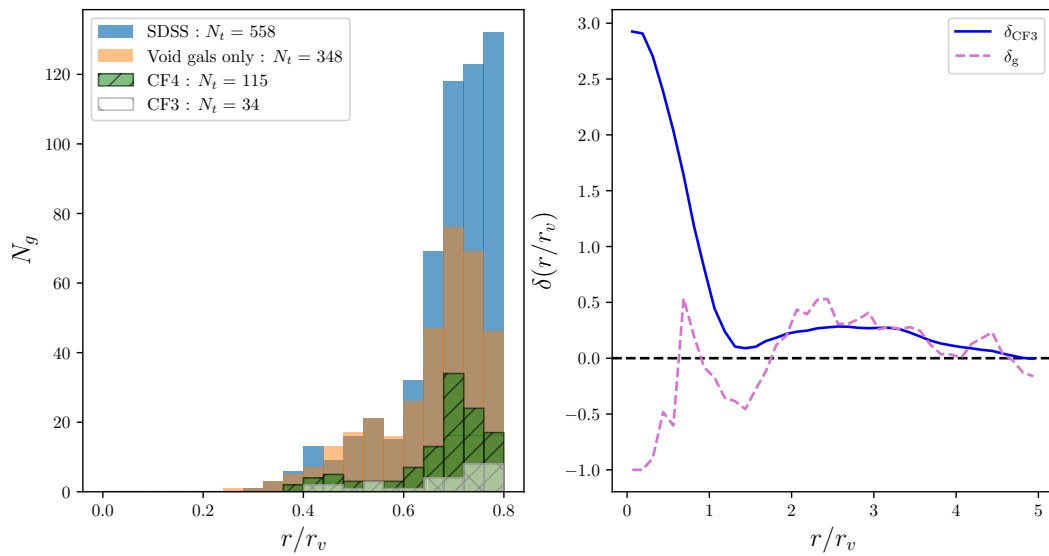
Void 487



Void 727



Void 738



Void 941

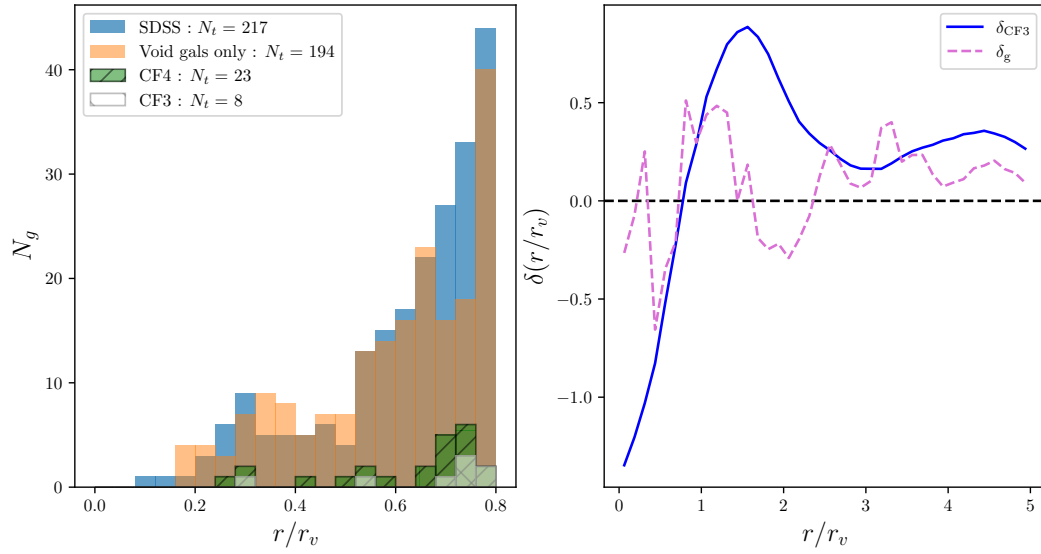


Fig. 4: Void radial density profiles. For each of the seven SDSS/CAVITY nearby voids that are included in the CosmicFlows-3 volume, we show the radial number of galaxies in the left panel and the matter content in the right panel computed from CF3 (blue) and from the galaxy number density in SDSS (pink). All seven voids are empty of galaxies near their center and roughly up to their effective radius. However, four voids (474, 487, 727 and 738) display CF3-computed overdensities of matter in their center.

Appendix A: Void density and velocity profiles

One may analytically compute the expected density and velocity profiles of isolated spherical voids, into the far nonlinear regime, up to the moment that voids experience shell crossing at their boundaries (for a review see van de Weygaert 2016). The explicit expression for the density and velocity profiles for an isolated spherical void may be found in Sheth & van de Weygaert (2004).

One major result is that voids have a characteristic density and evolution time, that of shell crossing. For a spherical void, this happens when it reaches a nonlinear density contrast $\delta \sim -0.8$ (i.e., 20% of the global cosmic density), by which time the void has expanded by a factor ~ 1.7 . This corresponds to a linear density contrast of $\delta_{lin} = -2.81$ (this is to be compared to the 1.69 for collapse of spherical overdensities).

A.1. Void density profiles

We may also use the expansion of isolated spherical voids to understand the overall density and velocity profiles of voids (see also van de Weygaert 2016) because they are underdense, they expand with respect to the background, and the interior shells expand faster than the outer ones. Due to the differential expansion of the interior mass shells, we see an accumulation of mass near the exterior and boundary of the void, meanwhile evening out the density distribution in the interior. This leads to a typical bucket-shaped density profile (opposite of top-hat), with a linear "Hubble-like" void flow in the interior (the canonical void is a "Hubble bubble"). For a wide range of initial radial profiles, voids will attain a bucket-shaped profile.

Recently, a range of studies have been published on the issue of void-density profiles, and the question of whether or not they display a universal behavior (see e.g., Hamaus et al. 2014; Cautun et al. 2016). For example, Ricciardelli et al. (2013) and Hamaus et al. (2014) concluded that spherically averaged den-

sity profiles of voids indeed imply a universal density profile that can be characterized by two parameters.

Interestingly, these density profiles have a less prominent bucket-shaped interior profile than those seen for the spherical voids. This may be understood from the fact that voids in general are not spherical, meaning that spherical averaging will lead to the mixing of different layers in the interior of a void. The recent study by Cautun et al. (2016) confirms this: when taking into account the shapes of voids, a remarkably strong bucket void density profile appears.

A.2. Void velocity profiles

In the situation of a mature, evolved void, the velocity field of a void resembles that of a Hubble flow, in which the outflow velocity increases linearly with distance to the void center. In other words, voids are super-Hubble bubbles (Icke 1984). The linear velocity increase is a reflection of the corresponding density distribution: the near constant velocity divergence within the void conforms to the near uniform bucket-shaped interior density distribution that voids attain at more advanced stages.

It is straightforward to appreciate this from the continuity equation. For a uniform density field, this equation tells us that the velocity divergence in the void will be uniform, corresponding to a Hubble-like outflow. Because voids are emptier than the rest of the Universe, they will expand faster, with a net velocity divergence equal to

$$\theta = \frac{\nabla \cdot \mathbf{v}}{H} = 3(\alpha - 1), \quad \alpha = H_{\text{void}}/H, \quad (\text{A.1})$$

where α is defined to be the ratio of the super-Hubble expansion rate of the void and the Hubble expansion of the Universe. van de Weygaert & van Kampen (1993) confirmed that the velocity outflow field in viable cosmological scenarios does indeed resemble that of a super-Hubble expanding bubble. These authors established that the super-Hubble expansion rate is directly proportional to the nonlinear void density $\Delta(t)$,

$$H_{\text{void}}/H = -\frac{1}{3}f(\Omega)\Delta(t). \quad (\text{A.2})$$

This relation, known within the context of a linearly evolving spherical density perturbation, in the case of fully evolved voids appears to be valid on the basis of the *nonlinear* void density deficit. Several studies (e.g., Hamaus et al. 2014) have confirmed this finding for voids in a range of high-resolution cosmological simulations. The immediate implication is that voids should be considered as distinctly *nonlinear* objects.

A.3. Nonspherical voids

One may wonder how far the nonsphericity of voids works out for their density and velocity profiles. Cautun et al. (2016) showed that this may severely influence the density and velocity profiles extracted for these voids and that spherical averaging may not always lead to a correct result. In the interpretation of the profiles presented in the main text, these effects will certainly play a role.

While the results above emanate from a rather unrealistic symmetric configuration —spherical, isolated— many studies have shown these to be rather representative for the major fully expanding voids in the galaxy distribution. There is also a good reason why this is so: following the shell-crossing phase, the expansion of voids slows down (Bertschinger 1985). It was this

realization that led Dubinski et al. (1993) to point out that the large voids in redshift surveys are to be mostly identified with the voids that at the current epoch are undergoing shell crossing.